

# Gamma irradiation resistance of early age Ba(OH)<sub>2</sub>-Na<sub>2</sub>SO<sub>4</sub>-slag cementitious grouts



Neda Mobasher<sup>a</sup>, Susan A. Bernal<sup>a,b</sup>, Hajime Kinoshita<sup>a,\*\*</sup>, John L. Provis<sup>a,\*</sup>

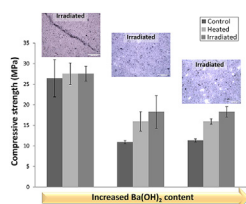
<sup>a</sup> Immobilisation Science Laboratory, Department of Materials Science & Engineering, The University of Sheffield, Sir Robert Hadfield Building, S1 3JD, United Kingdom

<sup>b</sup> Department of Civil & Structural Engineering, The University of Sheffield, Sir Frederick Mappin Building, S1 3JD, United Kingdom

## HIGHLIGHTS

- Ba(OH)<sub>2</sub>-Na<sub>2</sub>SO<sub>4</sub>-slag cements show gamma irradiation resistance.
- Sulfate-bearing wastes are immobilised in ettringite and BaSO<sub>4</sub> compounds.
- Ordering in C-A-S-H binder gel increases with gamma irradiation.

## GRAPHICAL ABSTRACT



## ARTICLE INFO

### Article history:

Received 28 May 2016

Received in revised form

13 October 2016

Accepted 19 October 2016

Available online 20 October 2016

### Keywords:

Gamma radiation

Nuclear waste

Barium sulfate

Alkali-activated cements

X-ray diffraction

Nuclear magnetic resonance spectroscopy

## ABSTRACT

The gamma irradiation resistance of early age Ba(OH)<sub>2</sub>-Na<sub>2</sub>SO<sub>4</sub>-slag cementitious grouts, formulated for the immobilisation of sulfate bearing nuclear waste, was assessed. The observable crystalline phases were not modified upon heating (50 °C) or upon gamma irradiation up to a total dose of 2.9 MGy over 256 h, but the compressive strengths of the irradiated samples increased significantly. <sup>27</sup>Al and <sup>29</sup>Si MAS NMR spectroscopy showed that the main binding phase, a calcium aluminosilicate hydrate (C-A-S-H) type gel, had a more ordered and polymerised structure upon heating and irradiation compared to that identified in reference samples. This is associated with a higher degree of reaction of the slag. Samples formulated with the waste simulant Na<sub>2</sub>SO<sub>4</sub>, but without Ba(OH)<sub>2</sub>, became porous and cracked upon heating and irradiation, but still retained their compressive strength. The Ba(OH)<sub>2</sub>-Na<sub>2</sub>SO<sub>4</sub>-slag grouts evaluated in this work withstand gamma irradiation without showing identifiable damage, and are thus a technically feasible solution for immobilisation of sulfate-bearing nuclear wastes.

© 2016 The Authors. Published by Elsevier B.V. This is an open access article under the CC BY license (<http://creativecommons.org/licenses/by/4.0/>).

## 1. Introduction

The immobilisation of sulfate bearing radioactive waste poses technical challenges for vitrification and traditional cementing processes. The presence of sulfate during vitrification causes phase separation in borosilicate glass [1], and in the case of Portland

cement-based materials it can promote microstructural changes in the long term [2–4], such as expansion and cracking through the process of internal sulfate attack, which may result in the loss of matrix integrity and the release of radionuclides into the environment. If sulfate-containing nuclear waste is not treated and encapsulated effectively, it can also interact with any Portland cement-based backfill or structural concrete used in a nuclear waste repository, potentially causing decay of the repository structure through sulfate attack processes.

Asano et al. [5] proposed a method for the solidification/stabilisation of sulfate-rich aqueous low level wastes using Ba(OH)<sub>2</sub> and blast furnace slag (BFS), derived from the iron making industry, via

\* Corresponding author.

\*\* Corresponding author.

E-mail addresses: [h.kinoshita@sheffield.ac.uk](mailto:h.kinoshita@sheffield.ac.uk) (H. Kinoshita), [j.provis@sheffield.ac.uk](mailto:j.provis@sheffield.ac.uk) (J.L. Provis).

a two-step process to produce cement-like solid monoliths. In their method, a sodium sulfate ( $\text{Na}_2\text{SO}_4$ ) (simulated waste) solution was mixed with  $\text{Ba}(\text{OH})_2$  in a first step, stabilising the sulfate ions through the precipitation of the highly insoluble phase barium sulfate ( $\text{BaSO}_4$ ) and releasing sodium hydroxide ( $\text{NaOH}$ ) as a by-product of this reaction. This was followed by a second step where the  $\text{BaSO}_4$  and  $\text{NaOH}$ -containing slurry was blended with slag to produce a cementitious grout.

Mobasher et al. [6] published a proof-of-concept of a one-step process to produce solid wasteforms with comparable chemistry to those assessed by Asano et al. [5] for immobilisation of sulfate bearing aqueous waste, formulating  $\text{Ba}(\text{OH})_2$ - $\text{Na}_2\text{SO}_4$ -BFS cementitious grouts. This study demonstrated that in the one-step process, in-situ precipitation of  $\text{BaSO}_4$  particles and chemical reaction between the slag and  $\text{NaOH}$  (also referred to as alkali-activation) take place simultaneously, with the remnant  $\text{Ba}(\text{OH})_2$  and  $\text{Na}_2\text{SO}_4$  interacting with the slag to form a hardened binder. A single-step approach has advantages from an operational point of view, compared with that proposed by Asano et al. [5], as reduced manipulation of the radioactive aqueous waste is desirable. Formation of barium sulfate in cementitious wasteforms is advantageous as it can enhance their radiation shielding properties due to the high atomic number of barium [7], and potentially promote co-precipitation of radionuclides such as  $^{90}\text{Sr}$  that can be present in the aqueous nuclear waste [8].

In our previous study,  $\text{Ba}(\text{OH})_2$ - $\text{Na}_2\text{SO}_4$ -slag composite wasteforms were characterised after six months of curing [9], and the results confirmed the formation of the low solubility salts  $\text{BaSO}_4$  and  $\text{BaCO}_3$  along with a calcium aluminosilicate hydrate (C-A-S-H) type phase, as the main reaction products. Calcium sulfoaluminate hydrates, most likely with some degree of barium substitution, and a hydrotalcite-type layered double hydroxide have been identified as secondary reaction products [10]. Both  $\text{Ba}(\text{OH})_2$ , and any residual  $\text{Na}_2\text{SO}_4$  that has not reacted with the  $\text{Ba}(\text{OH})_2$  to precipitate  $\text{BaSO}_4$ , aid the activation and therefore control the reaction of the slag. An increased content of  $\text{Ba}(\text{OH})_2$  promotes a higher degree of reaction, and the formation of a cross-linked C-A-S-H type gel.

Alkali-activated slag cements are produced via a chemical reaction between a source of alkalis (i.e. alkali activator) and blast furnace slag, producing hardened solids, if properly formulated and cured [10]. These binders have the potential to encapsulate radioisotopes and reactive metals, and when produced using sodium carbonate or sodium sulfate as alkali sources, develop a relatively moderate alkalinity compared with Portland cement based wasteforms [11]. In  $\text{Na}_2\text{SO}_4$ -activated slags, ettringite ( $\text{Ca}_6\text{Al}_2(\text{OH})_{12}(\text{SO}_4)_3 \cdot 26\text{H}_2\text{O}$ ) forms as a major crystalline reaction product, which chemically binds  $\text{SO}_4^{2-}$  present in the system, and can act as a host for a number of positively and negatively charged ions as isomorphous substituents within its structure [12], including various radionuclides.

As cementitious wasteforms are exposed to ionising radiation throughout their lifetime service, it is essential to understand the effects of radiation, and determine if they can withstand such service conditions. Gamma irradiation is the focus of the present study, being the most penetrating ionising radiation and more difficult to shield than alpha and beta radiation. Most of the studies evaluating gamma irradiation resistance of cementitious wasteforms [13,14] focus on hardened cements and concretes based solely on Portland cement (PC), and assess the effects of gamma irradiation on mechanical properties and physical deterioration.

The most significant interaction of gamma rays with cementitious materials is the radiolysis of pore water, resulting in  $\text{H}_2$  gas as a primary product and  $\text{H}_2\text{O}_2$  as a secondary product [15]. The process of radiolytic dehydration can cause pressurisation, spalling and micro-cracks in the cement matrix [16,17]. In PC-based

materials, increased formation of calcite has been observed in the aged concrete samples exposed to high doses of gamma radiation samples [18,19]. This is a consequence of the reaction of the radiolysis product  $\text{H}_2\text{O}_2$  with calcium-rich phases formed upon hydration of PC, such as portlandite ( $\text{Ca}(\text{OH})_2$ ), to form calcium peroxide octahydrate ( $\text{CaO}_2 \cdot 8\text{H}_2\text{O}$ ), which can then be converted to calcite ( $\text{CaCO}_3$ ) in presence of  $\text{CO}_2$ .

The specific chemistry of slag-blended cements can also lead to distinct behaviour under irradiation when compared to plain PC materials. Richardson et al. [20] evaluated the microstructure of a BFS-PC (9:1) cement at a dose rate of 10 kGy/h to a total dose of 87 MGy, over two years at 50 °C. The formation of additional ettringite in the irradiated samples was observed when compared to the control samples, indicating that gamma radiation may accelerate the oxidation of the sulfide ( $\text{S}^{2-}$ ) supplied by the slag, to form sulfates ( $\text{SO}_4^{2-}$ ) and promote further formation of ettringite. Palmer and Fairhall [21] reported that for a similar formulation, the pore solution chemistry was mainly unaffected by gamma irradiation, although at doses of ~10 MGy there was evidence of an escalation in sulfate concentrations consistent with the proposed mechanism of sulfide oxidation by radiolysis. Mobasher et al. [17] also assessed the gamma radiation resistance of an early age BFS-PC (9:1) cement, at a dose rate of 18.6 kGy/h for total dose of 4.77 MGy over 256 h at 50 °C. Cracks and open pores formed in the irradiated specimen as a result of radiolytic dehydration, but the strength was not compromised. Ettringite was preserved in the irradiated sample but absent from heated control samples. Craeye et al. [22] observed similar results regarding formation of ettringite under gamma irradiation for a BFS-rich cement mortar, but not in a plain PC system.

Haruguchi-Yukitomo et al. [23] carried out gamma-irradiation experiments (160 kGy total dose) in calcium aluminate composite grouts containing  $\text{Na}_2\text{SO}_4$  and  $\text{Ba}(\text{OH})_2$ , developed for the immobilisation of sodium sulfate wastes via precipitation of ettringite and  $\text{BaSO}_4$ . The results revealed a notable reduction in  $\text{H}_2$  gas generation in these composites, when compared with other cementitious grouts typically used by the nuclear industry (i.e. PC and PC/BFS), although this was strongly influenced by the desiccation rate of the calcium aluminate composites. The reduction in  $\text{H}_2$  generation was attributed to the low water saturation condition of the ettringite present in those cements.

The present study investigates the gamma irradiation resistance of two early-age  $\text{Ba}(\text{OH})_2$ - $\text{Na}_2\text{SO}_4$ -BFS composite cements (cured for only 8 days prior to irradiation), which have been developed as potential cementitious grouts for the immobilisation/encapsulation of sulfate bearing nuclear wastes. A sodium sulfate-activated slag was also evaluated for comparison purposes, and irradiated under similar conditions to the composite cements. The irradiation effects at early age are of particular interest because the cementitious wasteforms contain a significant amount of free water at this time, which can be subject to radiolysis and consequent  $\text{H}_2$  gas generation. As a result of gamma irradiation, heat is also generated. To investigate its effect, parallel samples were heat-treated (50 °C) for a length of time corresponding to the radiation exposure (256 h), and evaluated as a second control (in addition to unheated specimens) to distinguish the effects of elevated temperature from those associated solely with irradiation.

## 2. Experimental methods

### 2.1. Materials

A blast furnace slag (BFS) from Redcar, UK, with a Blaine fineness of 286  $\text{m}^2/\text{kg}$ , was used in this study. The chemical composition of the BFS is presented in Table 1. Barium hydroxide octahydrate

**Table 1**

Chemical composition of blast furnace slag (BFS), from X-ray fluorescence analysis. LOI is loss on ignition at 1000 °C.

Component as oxide	CaO	SiO <sub>2</sub>	Al <sub>2</sub> O <sub>3</sub>	Fe <sub>2</sub> O <sub>3</sub>	MgO	K <sub>2</sub> O	Na <sub>2</sub> O	SO <sub>3</sub>	others	LOI
Weight %	38.8	35.8	13.4	0.9	7.6	0.4	0.3	0.7	1.5	0.9

(Ba(OH)<sub>2</sub>·8H<sub>2</sub>O, 97% purity) and sodium sulfate (Na<sub>2</sub>SO<sub>4</sub>, 99% purity) from Alfa Aesar were also used. The particle size distribution of this slag, determined by laser diffraction, is shown in Fig. 1.

## 2.2. Sample formulation and testing

A simulated aqueous sulfate-bearing waste (10 wt% aqueous Na<sub>2</sub>SO<sub>4</sub>) was prepared by dissolving solid anhydrous Na<sub>2</sub>SO<sub>4</sub> (Sigma Aldrich, ≥99%) in distilled water at 40 °C, and then mixed with a homogeneous blend of unreacted BFS and powdered Ba(OH)<sub>2</sub>·8H<sub>2</sub>O (Sigma Aldrich, ≥98%) in a sealed plastic container. Detailed formulations of the paste specimens produced are given in Table 2. The samples were manually shaken for 2–5 min at room temperature, mixed for 5 more minutes using a Whirl Mixer, then poured into 50 mL plastic centrifuge tubes, which were then sealed and cured for 8 days at 20 °C.

After the curing period, the samples were de-moulded, cut into cylinders of 27 mm in diameter and 27 mm in height, and wrapped in aluminium foil. Samples were separated into three groups, each of which was treated in a specified environment prior to analysis:

- **Irradiated samples** were treated in the Dalton Cumbrian Facility with gamma radiation from a self-shielded <sup>60</sup>Co source. The specimens wrapped in aluminium foil were irradiated in air to the doses shown in Table 3 over 256 h.
- **Control samples** were wrapped in aluminium foil and kept at 20 °C in the laboratory for a time equivalent to the irradiation period before testing, which would provide a reference to understand behaviour of the materials including the natural desiccation if that is to occur.
- **Heated samples** were wrapped in aluminium foil and kept at 50 °C in air using an electric oven for a time equivalent to the irradiation period, before testing. This temperature was specified to match the average temperature of 50 ± 5 °C in the irradiation chamber during radiation exposure.

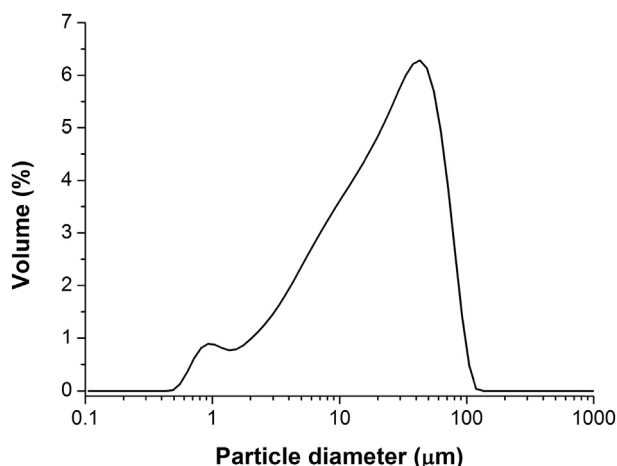


Fig. 1. Particle size distribution of anhydrous Redcar BFS.

## 2.3. Tests and analysis

After the exposure described in section 2.2, monolithic specimens were used for optical microscopic analysis first, and then compressive strength was measured. The crushed samples were immersed in acetone to arrest any residual hydration reaction processes. After 3 days, the samples were removed from the acetone, dried inside a vacuum desiccator for 24 h. These were then ground with an agate mortar and sieved to <63 μm using a brass sieve, for analysis by the following analytical techniques:

- X-ray diffraction (XRD) was conducted using a Siemens D5000 instrument (Cu K<sub>α1</sub>, λ = 1.54178 Å), with a step size of 0.02°, and a scanning speed of 0.5°/min between 5° and 55°.
- Solid-state <sup>29</sup>Si magic angle spinning (MAS) nuclear magnetic resonance (NMR) spectra were collected at 59.56 MHz on a Varian Unity Inova 300 (7.05 T) spectrometer using a probe for 7.5 mm o.d. zirconia rotors and a spinning speed of 5 kHz. The <sup>29</sup>Si MAS NMR employed a 90° pulse duration of 5 μs, a relaxation delay of 5 s, and 14,000 scans. Solid-state <sup>27</sup>Al MAS NMR spectra were acquired at 104.198 MHz, using a Varian VNMRs 400 (9.4 T) spectrometer and a probe for 4 mm o.d. zirconia rotors, a spinning speed of 14 kHz with a pulse width of 1 μs (approximately 25°), a relaxation delay of 0.2 s, and a minimum of 7000 scans. <sup>29</sup>Si and <sup>27</sup>Al chemical shifts are referenced to external samples of tetramethylsilane (TMS) and a 1.0 M aqueous solution of Al(NO<sub>3</sub>)<sub>3</sub>, respectively. All the spectra reported here were normalised to equal area for comparison.
- Thermogravimetric analysis (TG) was carried out using a Perkin Elmer Pyris 1 TGA. Approximately 40 mg of sample was heated at 10 °C/min in an alumina crucible under a nitrogen atmosphere (40 mL/min), between 25 °C and 950 °C.
- Microscopic inspection of solid samples was carried out using an optical microscope Nikon Eclipse LV150 with 50× magnification, with Buehler Omnimet Enterprise 9.5 software, to identify any large cracks forming in the specimens. Thresholding of the micrographs was carried out using ImageJ.
- Compressive strength of cylindrical specimens was measured using a Zwick Roell Z050 machine at a load rate of 0.5 mm/min. The results were corrected using a shape factor of 0.85 for cylinders of aspect ratio 1.0.

## 3. Results and discussion

### 3.1. X-ray diffraction

Fig. 2 illustrates X-ray diffractograms of control, heated and irradiated samples. All the samples show reflection peaks of crystalline åkermanite (Ca<sub>2</sub>MgSi<sub>2</sub>O<sub>7</sub>; Powder Diffraction File (PDF) #076-0841) and minor traces of calcite (CaCO<sub>3</sub>, PDF # 47-1743) contributed by the anhydrous slag. The diffractogram of the control M0 sample (Fig. 2A) presents reflections corresponding to ettringite ((CaO)<sub>3</sub>(Al<sub>2</sub>O<sub>3</sub>)(CaSO<sub>4</sub>)<sub>3</sub>·32H<sub>2</sub>O; PDF # 041-1451), which has been reported as one of the main crystalline reaction products in NaSO<sub>4</sub>-activated slag cements [24,25]. A broad diffuse hump between 22° and 37° 2θ is also identified, and assigned to a highly disordered Al-substituted calcium silicate hydrate (C-A-S-H) type gel, which is

**Table 2**

Formulations of  $\text{Na}_2\text{SO}_4$ -BFS and  $\text{Na}_2\text{SO}_4$ - $\text{Ba}(\text{OH})_2$ -BFS cements. The water/binder (w/b) ratio column includes water incorporated as part of the hydrous barium hydroxide, and the total solids (BFS +  $\text{Na}_2\text{SO}_4$  + anhydrous BaO contained in  $\text{Ba}(\text{OH})_2 \cdot 8\text{H}_2\text{O}$ ) are considered as ‘binder’ in this calculation.

Sample ID	$\text{Ba}^{2+}:\text{SO}_4^{2-}$ molar ratio	w/b	BFS (g)	$\text{H}_2\text{O}$ (g)	$\text{Na}_2\text{SO}_4$ (g)	$\text{Ba}(\text{OH})_2 \cdot 8\text{H}_2\text{O}$ (g)
M0	0:1.0	0.34	100	35	3.9	0
M1.0	1.0: 1.0	0.36	100	35	3.9	8.64
M1.3	1.3: 1.0	0.37	100	35	3.9	11.23

**Table 3**

Details of the gamma irradiation dose rate and total dose for samples.

Sample ID	Dose rate (kGy/h)	Total dose (MGy)
M0	10.3	2.65
M1.0	11.3	2.90
M1.3	11.5	2.95

typically identified as the main binding phase in alkali-activated slag cements [26]. Changes in the phase assemblage of the M0 sample upon heating or irradiation are not observed in the XRD results.

Fig. 2B and C show the XRD patterns for the  $\text{Ba}(\text{OH})_2$ -containing M1.0 and M1.3 samples, respectively. These grouts additionally present reflections corresponding to barite ( $\text{BaSO}_4$ ; PDF #24-1035) and witherite ( $\text{BaCO}_3$ ; PDF #45-1471), which demonstrate the effective interaction of the  $\text{Ba}(\text{OH})_2$  with sulfate species (and atmospheric carbonates) present in these systems, even at early ages of reaction. A broad diffuse scattering feature is also observed in the diffractograms of M1.0 and M1.3 samples, again assigned to a C-A-S-H type phase, consistent with samples produced with similar formulations assessed after six months of curing [25]. These cementitious grouts present a reflection at  $8.5^\circ 2\theta$ , which is shifted to a slightly lower  $2\theta$  value when compared to the main reflection peak of ettringite ( $9.0^\circ 2\theta$ ). This has been previously observed in these cements after 6 months of curing, and attributed to a Ba-containing ettringite type phase, which is likely to present a larger  $d$ -spacing than pure ettringite, inducing a peak shift to lower angle, as observed in these samples [27].

The M1.0 and M1.3 appear to contain less ettringite than M0, consistent with the fact that a significant fraction of the sulfate present precipitates as  $\text{BaSO}_4$ , and thus there is a reduced concentration of  $\text{SO}_4^{2-}$  species available for ettringite formation. A hydrogarnet type phase (resembling  $\text{Ca}_3\text{Al}_2(\text{OH})_{12}$ , PDF#24-0217, potentially with some Si substitution) is also observed. It has been reported that decomposition of monosulfoaluminate, at high temperatures and high pressure, leads to the formation of hydrogarnet type phases and bassanite ( $\text{CaSO}_4 \cdot \frac{1}{2}\text{H}_2\text{O}$ ) [28]. Utton et al. [29] identified a hydrogarnet type phase along with  $\text{BaSO}_4$  particles in PC/BFS grouts with added barium carbonate and cured at high temperature ( $60^\circ\text{C}$ ). The formation of the hydrogarnet was attributed to the decomposition of the monocarboaluminate phases present in the PC/BFS, induced by the presence of barium. In the  $\text{Ba}(\text{OH})_2$ -containing cementitious grouts studied here (i.e. M1.0 and M1.3 samples), crystalline monosulfoaluminate type phases were not identified by XRD, which might be a consequence of sulfate consumption by formation of  $\text{BaSO}_4$  leading instead to a preference for the hydrogarnet type phase identified.

The XRD patterns of the irradiated M1.0 and M1.3 samples (Fig. 2) do not show phase assemblage alteration compared to the respective control and heated specimens. This suggests that the crystalline reaction products formed at this early stage of reaction withstand gamma irradiation exposure, and irradiation or heating are not promoting changes in the phase assemblage.

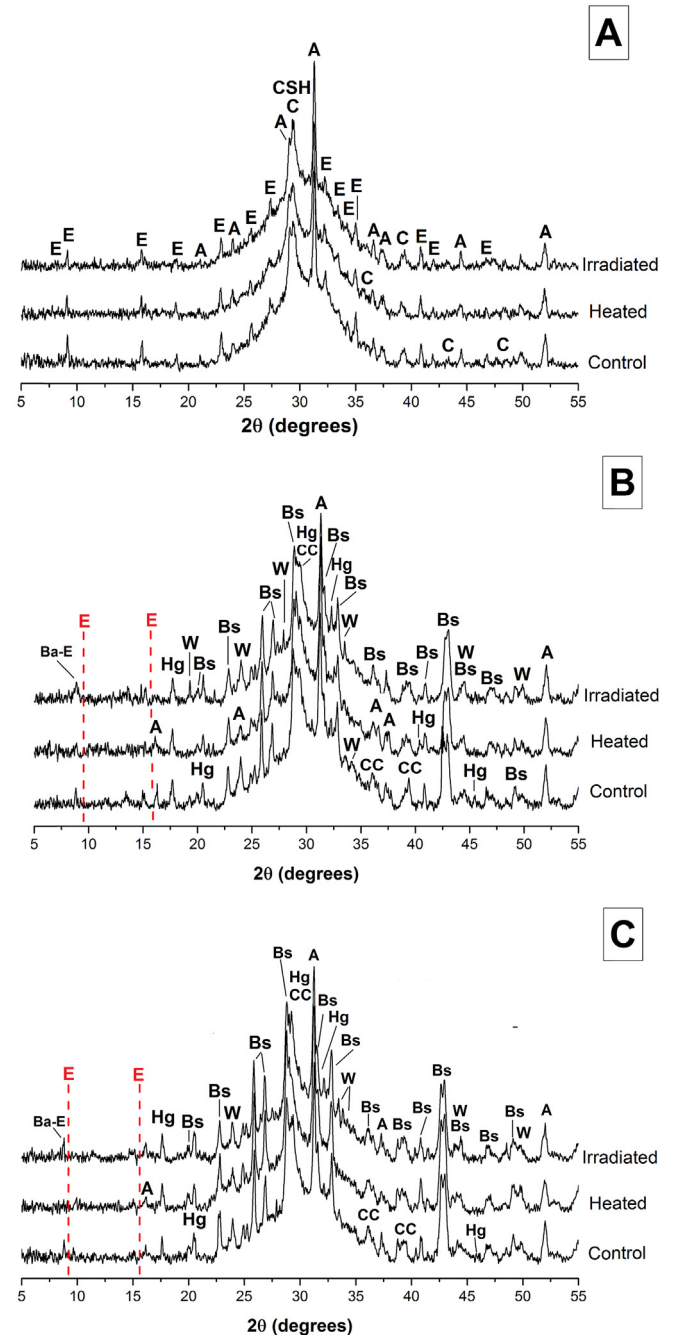


**Fig. 2.** X-ray diffractograms of control, heated and irradiated  $\text{Ba}(\text{OH})_2$ - $\text{Na}_2\text{SO}_4$ -slag cementitious grouts, with  $\text{Ba}^{2+}:\text{SO}_4^{2-}$  ratios: (A) M0, (B) M1.0 and (C) M1.3. Peaks marked correspond to åkermanite (A), calcite (CC), ettringite (E), barium-containing ettringite (Ba-E), barite (Bs), witherite (W), hydrogarnet (Hg), and Al-substituted calcium silicate hydrate (CSH). The vertical dashed lines in (B) and (C) indicate the original position of the (100) peak of ettringite.

### 3.2. Solid-state $^{27}\text{Al}$ MAS NMR spectroscopy

Solid-state MAS NMR spectroscopy is applied here to study the Al-rich reaction products, and also aluminium incorporation into the C-A-S-H type phase. Fig. 3 shows the solid state  $^{27}\text{Al}$  MAS NMR spectra of the anhydrous slag and samples M0, M1.0 and M1.3 following different exposure treatments.  $^{27}\text{Al}$  MAS NMR spectra of minerals and glasses can typically show three distinct aluminium coordination environments ( $\text{Al}^{(\text{IV})}$ ,  $\text{Al}^{(\text{V})}$  and  $\text{Al}^{(\text{VI})}$ ), which are located at chemical shifts of 50–80 ppm, 30–50 ppm and –10 to 30 ppm, respectively [30]. The unreacted slag shows a broad resonance between 40 and 80 ppm, centred around 60 ppm. This region is assigned to tetrahedral Al environments, but cannot be assigned to a well-defined single site type due to structural disorder in the slag. This broad peak is attributed to the glassy phases which comprise the majority of the BFS.

The M0 samples (Fig. 3A) display two high intensity resonance peaks in the region associated with octahedrally coordinated Al (–10 to 30 ppm). The peak centred at 13 ppm is assigned to ettringite [31], in agreement with the XRD results for these samples (Fig. 2A). This resonance is slightly less intense in the M0 sample heated at 50 °C, compared with the control and irradiated samples, consistent with an increase in the intensity of the resonance at 9.5 ppm, assigned to Ca-Al or Mg-Al layered double hydroxide (LDH) type phases [31,32], for instance the ‘alumino-ferrite-mono’ (AFm) family of calcium aluminate hydrates which are often intermixed with C-A-S-H in slag-based cements [33–35]. Several studies report the formation of AFm-structured monosulfoaluminate at the expense of ettringite at 50 °C [36–39], which is particularly favoured in cement systems with high concentrations of alkalis and limited availability of  $\text{SO}_4^{2-}$  [40]. The stability of ettringite decreased due to its increased solubility at increased temperature, resulting in its partial conversion to the AFm phase [40], although higher concentrations of sulfates in the cements aid ettringite to persist at increased temperatures [41]. LDH type

phases were not identified in the XRD results in Fig. 2; this indicates that these phases are mainly present in a crystallographically disordered state, and are most likely either intermixed with the C-A-S-H products or present in amounts too small to be detected by X-ray diffraction.

The band assigned to ettringite in the irradiated M0 has a comparable intensity to that identified for the control sample, which indicates that the gamma irradiation is not destabilising the ettringite. This is consistent with the observations of Richardson et al. [20], Mobasher et al. [17] and Craeye et al. [22] for BFS-rich Portland cement blends. In BFS-PC grouts, Richardson et al. [20] proposed that radiolytic oxidation of the sulfide supplied by the BFS to sulfate is likely to take place, and this increases the concentration of sulfates sufficiently to stabilise ettringite, even at the elevated temperature reached during gamma irradiation.

For samples M1.0 (Fig. 3B) and M1.3 (Fig. 3C) (control, heated and irradiated), the octahedral Al region is dominated by a sole peak at 10.5 ppm that cannot be assigned to a single phase, but most likely corresponds to resonances of the poorly crystalline LDH phases present in these grouts, along with the contribution of the ettringite observed in these samples by XRD (Fig. 2B and C). The hydrogarnet phase identified in the samples M1.0 and M1.3 by XRD is likely to provide some additional intensity on the higher chemical-shift side of this dominant peak, as it resonates ~1–2 ppm downfield of the peak assigned to the LDH phases [42]. There is no identifiable change in the octahedral Al resonances, as a result of either heating or irradiation of the samples, indicating a high degree of nanostructural stability of the Al-rich phases upon gamma irradiation.

For all the cementitious grouts studied, in the region corresponding to tetrahedrally coordinated Al (80–50 ppm), formation of two distinct sites at 74 and 64 ppm is observed, which correspond to the different sites where substitution of Al into the C-A-S-H type phase occurs, and the fraction of unreacted slag still present in the grouts [43]. For M0 (Fig. 3A) the tetrahedral band is more

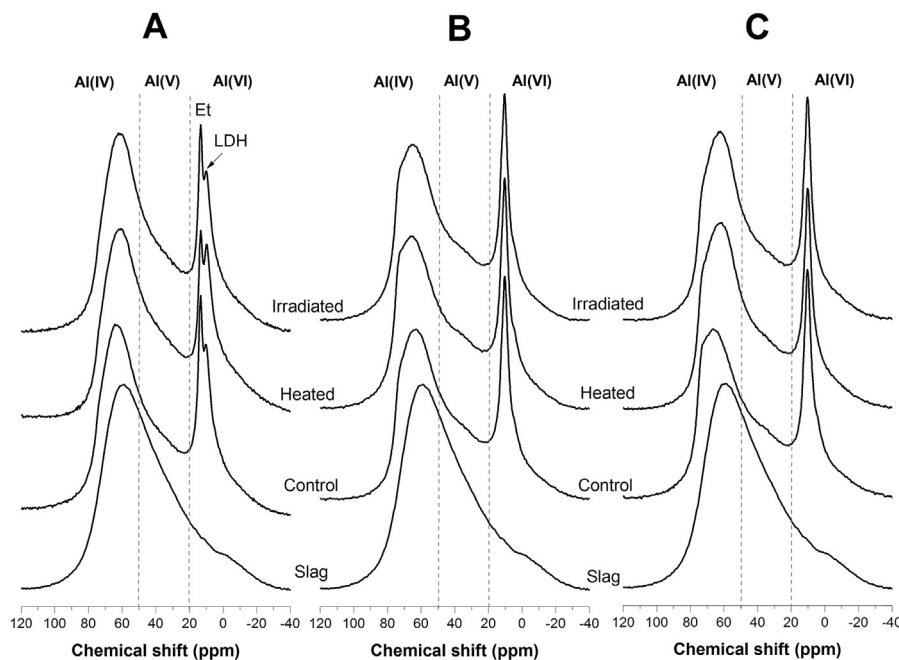


**Fig. 3.** Solid-state  $^{27}\text{Al}$  MAS NMR spectra of hardened  $\text{Ba}(\text{OH})_2\text{-Na}_2\text{SO}_4\text{-slag}$  cementitious grouts, with  $\text{Ba}^{2+}:\text{SO}_4^{2-}$  ratios (A) M0, (B) M1.0 and (C) M1.3, after different exposure conditions. Approximate regions of three aluminium coordination environments ( $\text{Al}^{(\text{IV})}$ ,  $\text{Al}^{(\text{V})}$  and  $\text{Al}^{(\text{VI})}$ ) are also indicated as a guide in the figure. In the  $\text{Al}^{(\text{VI})}$  region in (A), peaks are marked for ettringite (Et) and layered double hydroxide (LDH) structures.

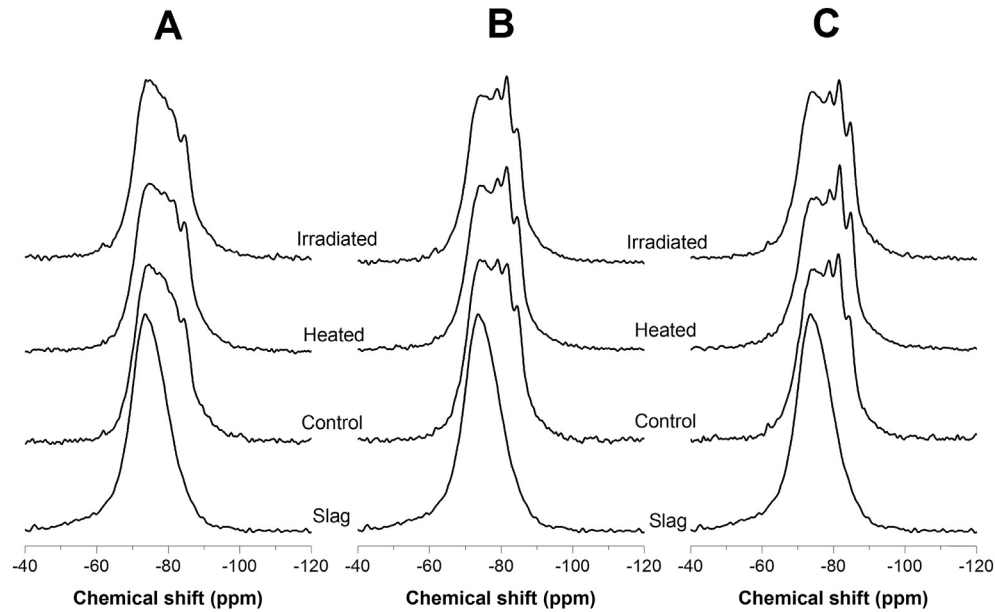


**Fig. 4.** Solid-state  $^{29}\text{Si}$  MAS NMR spectra of hardened  $\text{Ba}(\text{OH})_2\text{-Na}_2\text{SO}_4\text{-slag}$  cementitious grouts, with  $\text{Ba}^{2+}:\text{SO}_4^{2-}$  ratios (A) M0, (B) M1.0 and (C) M1.3, after different exposure conditions.

asymmetric and broader in the heated and irradiated samples than in the control sample, particularly in the region between 60 and 40 ppm, which might indicate the formation of a more cross-linked Al substituted C-A-S-H type phase in these samples, corresponding to the known increase in C-A-S-H crosslinking at higher temperature [44]. For M1.0 and M1.3 (Fig. 3B and C), following heat and irradiation treatment, the intensity of the tetrahedral Al region is slightly higher than in the control samples. This indicates a higher content of Al in the C-A-S-H type phase following exposure. This will be addressed in detail in section 3.3 in terms of the overall extent of reaction of the slag.

### 3.3. Solid-state $^{29}\text{Si}$ MAS NMR spectroscopy

Solid-state  $^{29}\text{Si}$  MAS NMR spectroscopy is applied in this work particularly to study the structure of the C-A-S-H type phase. Fig. 4 illustrates the spectra obtained for the M0, M1.0 and M1.3 specimens. The unreacted slag has a broad and featureless line shape, centred at  $-74$  ppm, indicating a highly disordered structure. In all the activated samples, resonances between  $-80$  ppm and  $-90$  ppm are identified, consistent with the formation of a C-A-S-H type phase, as identified in similar grouts after six months of curing [9]. In particular, distinct peaks centred at  $-82$  ppm and  $-84$  ppm corresponding to  $\text{Q}^2(1\text{Al})$  and  $\text{Q}^2$  sites respectively, are assigned to the Al-substituted C-S-H type gel with a tobermorite type structure [35,45].

The spectrum of the M0 control sample (Fig. 4A) shows mainly the contribution of the unreacted slag, along with a minor increase in intensity in the region attributable to  $\text{Q}^2(1\text{Al})$  and  $\text{Q}^2$  sites but with barely resolvable peaks, which indicates limited formation of a C-A-S-H type phase in this sample at early age (8 days of curing). Assessment of this cementitious formulation by isothermal calorimetry [46] revealed that the main acceleration-deceleration process, associated with the nucleation, growth and precipitation of reaction products takes place between 3 and 10 days after mixing. Therefore, the extent of reaction of the slag of the M0 samples is expected to be low. These results are also in agreement with the  $^{27}\text{Al}$  MAS NMR results discussed in section 3.2.

Upon heating of the M0 sample (Fig. 4A) a slight increase in intensity in the  $\text{Q}^2(1\text{Al})$  and  $\text{Q}^2$  sites is observed, indicating that this thermal treatment is accelerating the reaction of slag in this cement, favouring the formation of C-A-S-H type gel, compared with the control sample. Conversely, the  $^{29}\text{Si}$  MAS NMR spectrum of

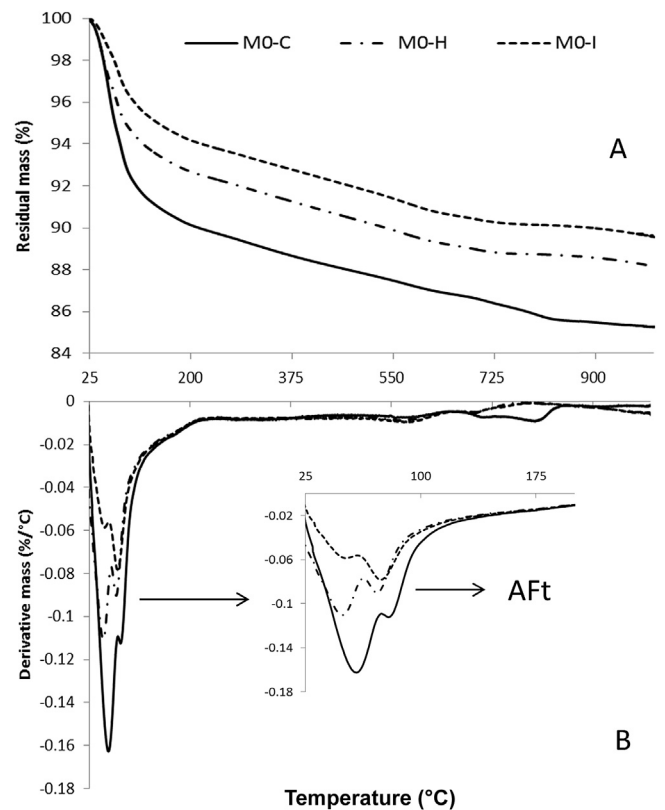


**Fig. 5.** Thermograms (A) and differential thermograms (B) (mass loss downwards) of the control (M0-C), heated (M0-H) and irradiated (M0-I) M0 samples. Low-temperature region highlighting the ettringite peak is shown as an inset on (B).

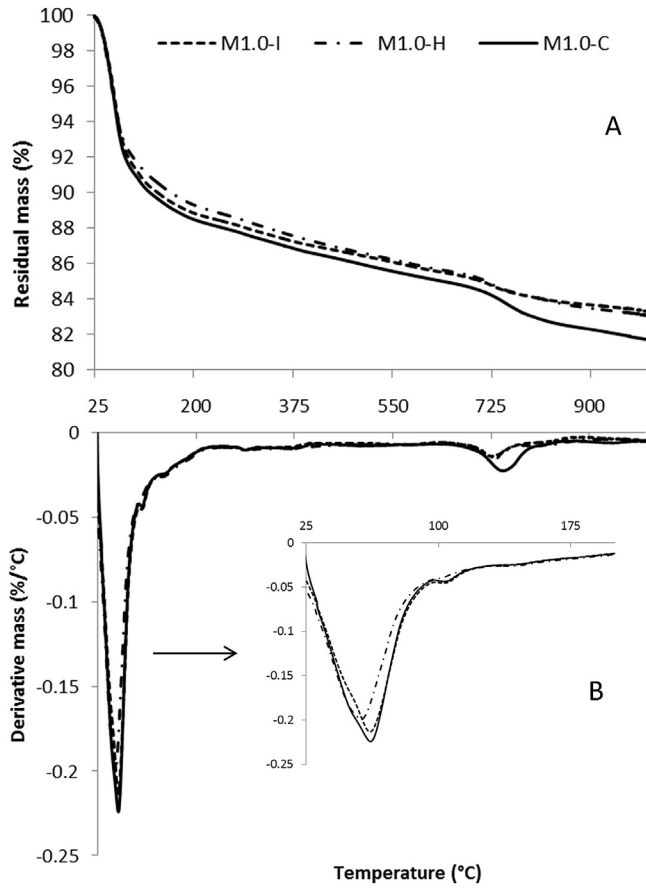


Fig. 6. Thermograms (A) and differential thermograms (B) (mass loss downwards) of the control (M1.0-C), heated (M1.0-H) and irradiated (M1.0-I) M1.0 samples.

the irradiated M0 sample does not display this change in the intensity of the  $Q^2$  sites, as it more closely resembles the spectrum of the control sample.

In the control M1.0 and M1.3 samples, Fig. 4B and C respectively, well-resolved bands corresponding to  $Q^1$  (centred at  $-80$  ppm),  $Q^2(Al)$  and  $Q^2$  sites corresponding to the C-A-S-H type phase are observed, with intensities significantly higher than those of the M0 control sample (Fig. 4A). Similar results were observed in these cements after extended curing (6 months) [9], where the added  $Ba(OH)_2$  that is not yet consumed upon formation of  $BaSO_4$  is able to act as an activator and promotes a higher extent of reaction of the slag, as it raises the alkalinity of the system compared with the use of sodium sulfate as the sole activator. The intensities of the  $Q^2(1Al)$  and  $Q^2$  sites are slightly higher in the control M1.3 pastes compared with control M1.0 grouts, consistent with the greater  $Ba(OH)_2$  addition yielding additional C-A-S-H type products.

The intensities of the  $Q^2(1Al)$  and  $Q^2$  sites observed in the heated and irradiated M1.0 and M1.3 samples are higher than those of the respective controls, indicating an increase in the content and/or degree of polymerisation of the C-A-S-H phase forming in these binders. The component peaks for each of these sites are also sharp, corresponding to a relatively high degree of nanostructural ordering within the long-range-disordered C-A-S-H type gel. As was discussed in section 3.2, the effect of temperature can be significant in determining the ordering, polymerisation and any possible cross-linking of the C-A-S-H type phase. There may be more Al available for incorporation into C-A-S-H in the heated samples as a result of partial decomposition of ettringite, as identified in the  $^{27}Al$  MAS NMR results. Conversely, as ettringite is

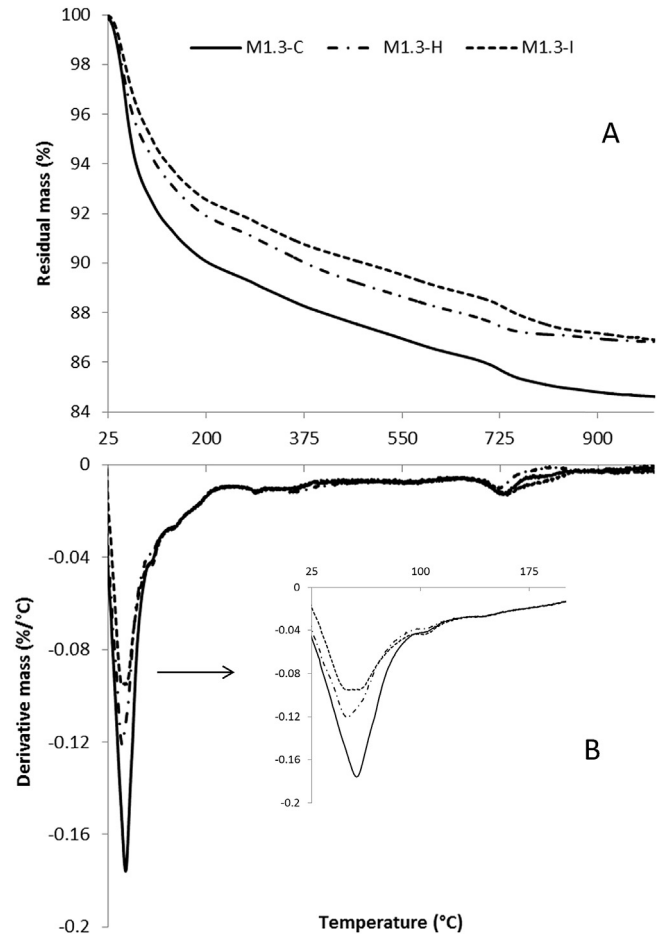


Fig. 7. Thermograms (A) and differential thermograms (B) (mass loss downwards) of the control, heated and irradiated M1.3 samples.

stabilised in the control and irradiated samples, less Al is accessible to be integrated in the C-A-S-H phases in these cases. The increased temperatures in the heated and irradiated samples may also potentially promote dissolution of the slag to provide the soluble species required for the formation of hydrate products to proceed.

There is no identifiable specific  $Q^3$  or  $Q^3(1Al)$  peak, typically reported at  $-89$  and  $-93$  ppm, respectively, in alkali-activated slag binders [47], which would enable unequivocal identification of a crosslinked tobermorite-like structure. However, the presence of a small contribution in this spectral region also cannot be fully discounted on the basis of the spectra collected at such a low extent of

Table 4

Mass loss of  $Ba(OH)_2$ - $Na_2SO_4$ -slag cementitious grouts determined from TGA, in specific temperature regions (%).

Sample ID	Exposure condition	Temperature range (°C)			
		25–100	100–500	500–800	25–1000
M0	Control	7.7	4.4	2.6	14.7
	Heated	5.4	4.2	2.2	11.8
	Irradiated	3.9	4.3	2.3	10.5
M1.0	Control	9.1	4.4	4.3	17.8
	Heated	8.3	4.2	3.6	16.1
	Irradiated	8.8	4.3	3.2	16.3
M1.3	Control	7.3	5.3	2.7	15.3
	Heated	5.5	5.4	2.2	13.1
	Irradiated	4.8	5.3	2.9	13.0

reaction.

### 3.4. Thermogravimetric analysis

Fig. 5 presents the thermograms and differential thermograms of M0 control, heated and irradiated samples. It has been reported for this sodium sulfate activated slag cement [25], that as a consequence of a relatively slow hydration process, there is a large amount of loosely bound water present in this system at early age. This water is observed in TG as mass lost below 100 °C, and can be affected by heat and irradiation. It appears that the irradiated sample contains less loosely bonded water than the heated one, which can be a result of the combined effect of dehydration during heating (which should be similar in both samples), and also radiolytic dehydration. The total mass loss up to 100 °C was 3.9% for the irradiated sample, 5.4% for the heated sample and 7.7% for the control sample.

There is an additional distinctive peak identified in the differential thermogravimetry (DTG) for the M0 control sample (Fig. 5B) below 100 °C, which is assigned to the dehydration of ettringite

[48] and the C-A-S-H type gel [49], which were identified as the main reaction product in this sulfate rich system via XRD and <sup>27</sup>Al MAS NMR (Figs. 2 and 3, respectively). There is no distinct peak identified for any AFm phase in the heated sample in Fig. 5B, consistent with the disordered nature and/or low content of the AFm components in these cements as noted by their absence from the XRD results. For the irradiated sample, the peak associated with ettringite appears more prominent, in agreement with the <sup>27</sup>Al MAS NMR results.

The thermograms and differential thermograms of M1.0 control, heated and irradiated samples are shown in Fig. 6. The total mass loss up to 100 °C was 8.8% for the irradiated sample, 8.3% for the heated sample and 9.1% for the control, indicating that there was little influence of the exposure conditions on the free water content of this cement. The ettringite peak at around 100 °C (inset, Fig. 6B) is notably weaker than in M0 (Fig. 5B), consistent with the results identified by XRD (Fig. 2B).

Fig. 7 illustrates the thermograms and differential thermograms of M1.3 control, heated and irradiated samples. The total mass loss up to 100 °C was 4.8% for the irradiated sample, 5.5% for the heated

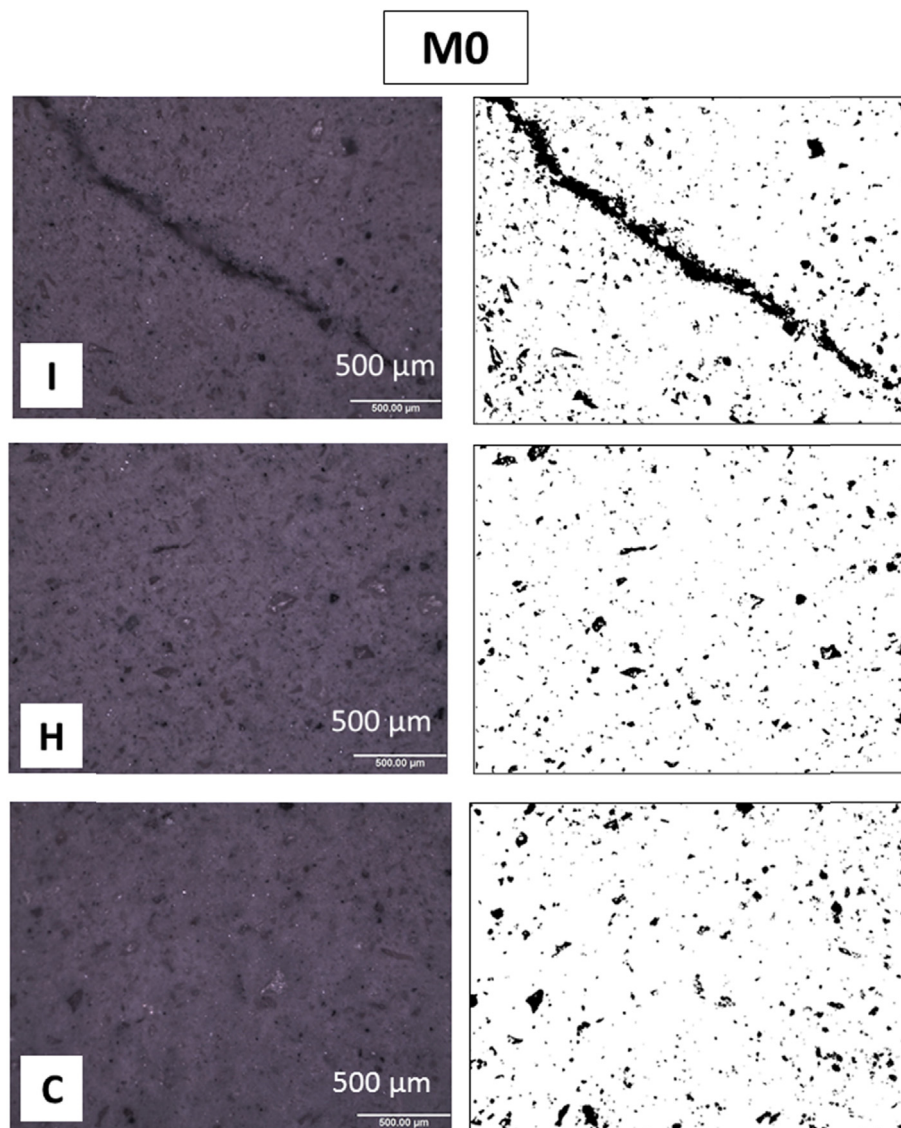


Fig. 8. Optical micrographs of (I) irradiated, (H) heated and (C) control specimens of Ba(OH)<sub>2</sub>-Na<sub>2</sub>SO<sub>4</sub>-slag cementitious grouts (M0) and corresponding thresholded images showing pores (black) and solid (white) regions.

sample and 7.3% for the control sample. This mass loss in the irradiated M1.3 cement is larger than in irradiated M1.0 (which may be linked to the slightly higher overall water/solids ratio in M1.3, Table 2), but still lower than irradiated M0. The ettringite peak is barely discernible in Fig. 6B, in good agreement with the XRD results (Fig. 2C).

Table 4 summarises the mass lost by each sample in specified temperature regions during the thermogravimetric analysis. The mass loss observed within these temperatures is associated with the release of loosely bound water from the specimens (<100 °C), the initial dehydration of the C-A-S-H and other hydrate phases, and also calcite decomposition [50]. BaCO<sub>3</sub> and BaSO<sub>4</sub> are not expected to decompose within the temperature range studied here.

The mass loss between 100 °C and 500 °C is associated with overlapping decomposition processes of C-A-S-H, LDH and hydrogarnet phases; the dehydration of the C-A-S-H phase is also largely complete by 500 °C [44,51,52]. It can be concluded from Table 4 that in the region of 100 °C–500 °C for each formulation, the irradiated and heated samples do not behave significantly differently from the respective control samples. Sample M1.3 has a higher mass loss in

this temperature range compared with M0 and M1.0, related to the formation of a larger amount of C-A-S-H type gel, consistent with an increased content of Ba(OH)<sub>2</sub>.

The mass loss associated with calcite decarbonation appears in the data at 500–800 °C [53]. Formation of calcite has been reported for PC samples upon gamma irradiation [18,19], related to the carbonation of hydration products (particularly Ca(OH)<sub>2</sub> in unmodified PC) and radiolysis products (e.g. CaO<sub>2</sub>·8H<sub>2</sub>O) [54]. However, Ca(OH)<sub>2</sub> is not present in the Na<sub>2</sub>SO<sub>4</sub>-BFS and Ba(OH)<sub>2</sub>-Na<sub>2</sub>SO<sub>4</sub>-BFS cements studied here. As shown in Table 4, there is no alteration observed in the mass loss associated with calcite due to irradiation, indicating that there is no additional calcite formation due to irradiation in the samples assessed.

### 3.5. Microscopic inspection

Figs. 8–10 present representative optical micrographs of the evaluated samples and the corresponding thresholded images, showing open macropores (in black) and solid regions (in white). The relatively large macropores observed in all the samples are

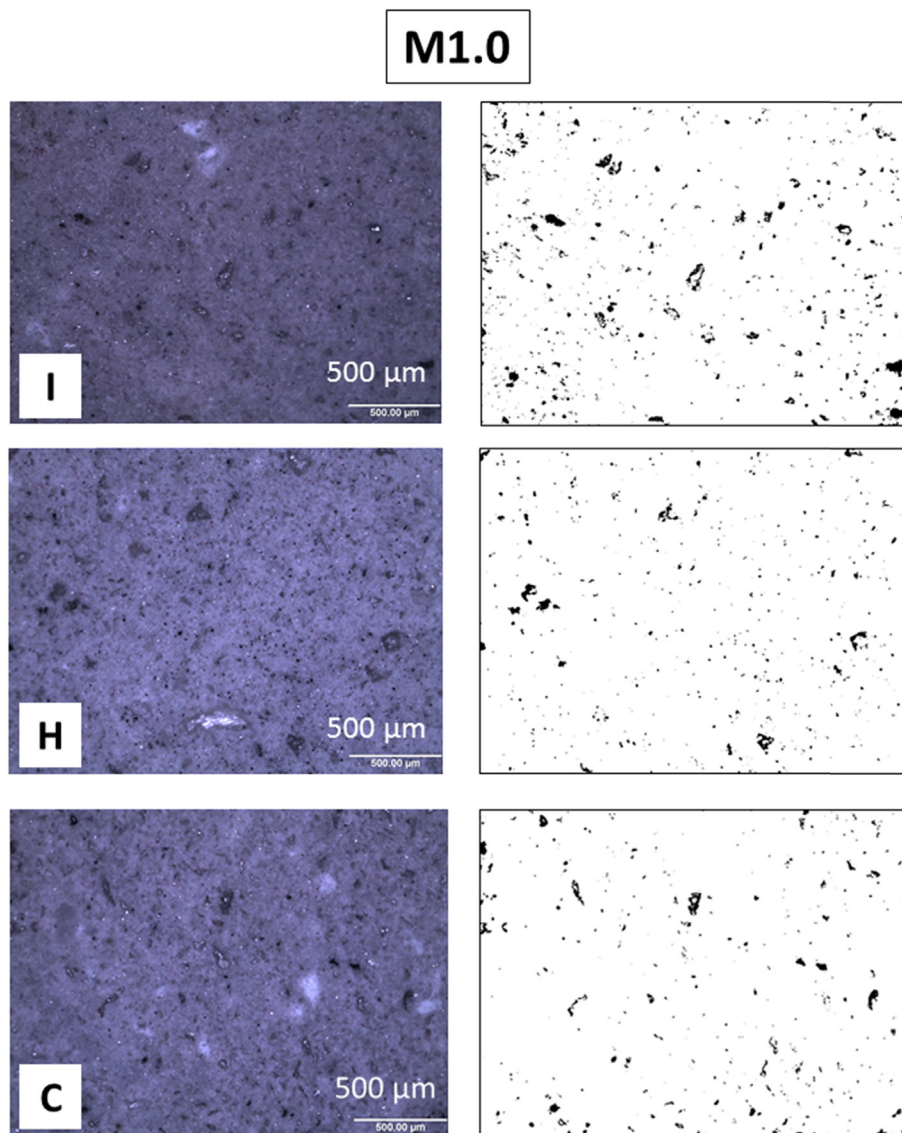


Fig. 9. Optical micrographs of (I) irradiated, (H) heated and (C) control specimens of Ba(OH)<sub>2</sub>-Na<sub>2</sub>SO<sub>4</sub>-slag cementitious grouts (M1.0), and corresponding thresholded images showing pores (black) and solid (white) regions.

likely to be associated with the air entrapped during mixing and paste casting.

Fig. 8 shows, for M0, that the irradiated sample (I) has more macropores and cracks compared with the heated (H) and control (C) samples. As discussed in section 3.4, the irradiated M0 sample (Fig. 5) had a significantly reduced content of loosely bound water compared with the heated and control samples. This elucidates that the dehydration mechanisms in the irradiation and heat treatments are different, resulting in the microstructural differences which are observable here. For slag-rich blends such as the 9:1 BFS-PC system, it has been proposed that the process of micro-crack formation upon irradiation is a consequence of pressurisation of the radiolytic gases inside the cement matrix, which leads to its collapse [16,17].

Fig. 9 shows typical optical micrographs of M1.0 samples. All the specimens appear largely similar, although the irradiated sample (I) has slightly more open pores than the heated (H) and control (C) samples. As identified by TGA (Table 4), the water loss values of M1.0 irradiated, heated and control samples were only slightly different, but were all significantly larger than in the corresponding M0 samples. Although more loosely bound water in the system

should lead to higher radiolysis upon irradiation exposure, micro-cracks were not observed in the M1.0 irradiated sample. Therefore, it appears that if the radiolysis of loosely bound water is occurring in this cementitious grout, it is not inducing the microcracking of the hardened monolith. Fig. 10 shows typical optical micrographs of M1.3 samples, which are very similar to the corresponding images of M1.0. Despite the slightly higher overall water content of the M1.3 sample in the original formulation (although lower free water), the structure of the irradiated sample appears unmodified.

The inclusion of  $\text{Ba}(\text{OH})_2$  in sodium sulfate activated slag cements induces significant changes in the phase assemblage, as identified by XRD (Fig. 1). In the context of radiation resistance of the wasteforms based on these cements, the most relevant difference between the M0 (without barium) and the barium-containing M1.0 and M1.3 samples is the formation of insoluble barium rich phases including barium sulfate (barite), which is used widely for the production of structural concrete in nuclear reactors to aid in radiation shielding [7,55]. The formation of  $\text{BaSO}_4$  in  $\text{Ba}(\text{OH})_2$ - $\text{Na}_2\text{SO}_4$ -BFS cements is likely to contribute to enhancement of the radiation resistance, by absorbing the radiation and thus restricting

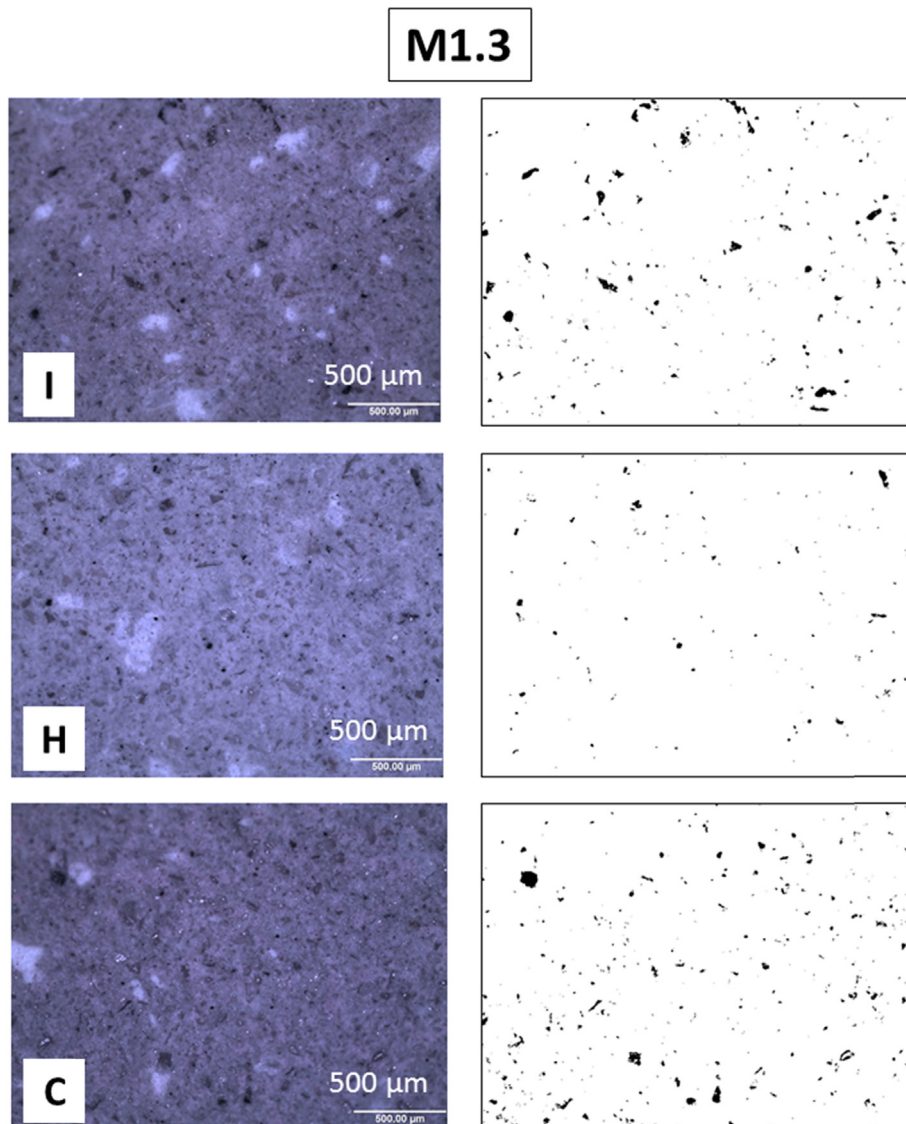


Fig. 10. Optical micrographs of (I) irradiated, (H) heated and (C) control specimens of  $\text{Ba}(\text{OH})_2$ - $\text{Na}_2\text{SO}_4$ -slag cementitious grouts (M1.3), and corresponding thresholded images showing pores (black) and solid (white) regions.

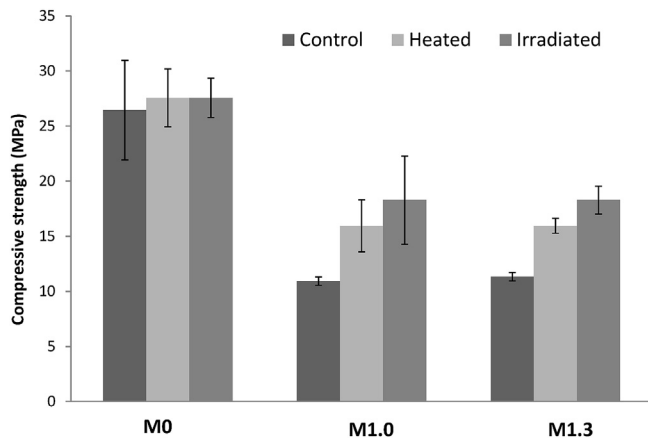


Fig. 11. Compressive strengths of  $\text{Ba}(\text{OH})_2\text{-Na}_2\text{SO}_4\text{-slag}$  cementitious grouts M0, M1.0 and M1.3. Error bars show one standard deviation of three replicate measurements.

the likelihood of interaction between photons and the water in the interior of the specimens.

### 3.6. Compressive strength

Fig. 11 shows the compressive strengths of the samples studied. The M0 system developed a higher compressive strength than the  $\text{Ba}(\text{OH})_2\text{-Na}_2\text{SO}_4\text{-BFS}$  composite grout. The early compressive strength of the M0 cement is attributed mainly to the formation of ettringite and also the initial stages of formation of C-A-S-H type gel. In M0, the compressive strengths of the control, heated and irradiated samples are comparable within the testing error, and above 25 MPa when measured using the small paste samples evaluated here. Although the irradiated M0 sample has lost a significant amount of loosely bound water (Table 4), resulting in large pores and cracks, the compressive strength of this sample is retained.

For samples M1.0 and M1.3, there is a significant rise in the compressive strength of the heated samples compared to the control samples, associated with the higher degree of reaction of the slag at increased temperature. For these formulations the irradiated samples had a slightly higher compressive strength than the heated samples. It was also observed in the  $^{27}\text{Al}$  and  $^{29}\text{Si}$  MAS NMR results (Figs. 3 and 4) that the structure of the C-A-S-H phase was modified, so that in the irradiated samples a more ordered and polymerised C-A-S-H gel was identified. This mechanism appears not to be taking place in the M0 sample, which neither gains nor loses strength, although Fig. 8 shows that it developed significant cracking during irradiation.

Further investigation is required to elucidate the mechanisms leading to the strength development of irradiated cementitious grouts at early stages of reaction. However, most significantly, the results presented here show that cements in the  $\text{Ba}(\text{OH})_2\text{-Na}_2\text{SO}_4\text{-BFS}$  system can retain, and in fact improve, in mechanical strength upon early-age gamma irradiation.

## 4. Conclusions

The effects of gamma irradiation in early-age  $\text{Ba}(\text{OH})_2\text{-Na}_2\text{SO}_4\text{-BFS}$  cementitious grouts and sodium sulfate activated slag cements were studied. The XRD results for all the irradiated samples show that  $\text{SO}_4^{2-}$  is chemically bound in the reaction products forming in these binders, particularly in  $\text{BaSO}_4$  and ettringite. No significant difference induced by heating or irradiation, compared to the control specimens, were identified. This suggests that the

crystalline reaction products formed at this early stage of reaction are able to withstand gamma irradiation exposure. The cements without  $\text{Ba}(\text{OH})_2$  contain a significant quantity of ettringite, while this phase is much less prominent in the  $\text{Ba}(\text{OH})_2$ -containing materials. Ettringite formation appears to be favoured by irradiation, consistent with the mechanism proposed in the literature that the oxidation of sulfide (from the slag) to sulfate can stabilise this phase at elevated temperatures. In the sodium sulfate activated slag cement with no addition of  $\text{Ba}(\text{OH})_2$ , as the activator has a near neutral pH, there is a large amount of loosely bound water within the samples at the early curing age tested. This formulation is the most susceptible to dehydration through heating and irradiation, which can result in formation of porosity and microcracking, although without evident loss of compressive strength.

For  $\text{Ba}(\text{OH})_2\text{-Na}_2\text{SO}_4\text{-BFS}$  cements, NMR spectra indicate a higher degree of reaction is due to the presence of  $\text{Ba}(\text{OH})_2$ , which increases the pH and promotes the dissolution of the slag. This leads to the formation of a relatively ordered C-A-S-H binding gel, as well as layered double hydroxide products, and at most a small amount of ettringite. In these systems the predominant mechanism of immobilisation of  $\text{SO}_4^{2-}$  is via formation of the insoluble salt  $\text{BaSO}_4$ . The degree of reaction also seems to be increased with the presence of heat and irradiation, resulting in a higher compressive strength compared to the unexposed control samples. These cements appear to be stable under the irradiation conditions used here (2.9 MGy over 256 h) as they retain their essential chemical stability, and do not show any cracks or structural modifications after irradiation. These results indicate that the  $\text{BaSO}_4$  forming in the  $\text{Ba}(\text{OH})_2\text{-Na}_2\text{SO}_4\text{-BFS}$  binders might be playing an important role in providing radiation resistance through attenuation of gamma radiation.

## Acknowledgements

This study has been sponsored by EPSRC through the University of Sheffield/University of Manchester Doctoral Training Centre 'Nuclear FiRST', EP/L015390/1. Participation of HK and JLP was partially sponsored by EPSRC through grant EP/N017684/1. The NMR spectra were collected using the EPSRC UK National Solid-state NMR Service at Durham University, and the assistance of Dr David Apperley is gratefully acknowledged. Special thanks are due to Dr Ruth Edge and Dalton Cumbrian Facility for their great assistance in the irradiation experiments. This study was performed, in part, at the MIDAS Facility, at the University of Sheffield, which was established with support from the Department of Energy and Climate Change.

## References

- [1] P.A. Bingham, R.J. Hand, Sulphate incorporation and glass formation in phosphate systems for nuclear and toxic waste immobilization, *Mater. Res. Bull.* 43 (7) (2008) 1679–1693.
- [2] R.S. Gollop, H.F.W. Taylor, Microstructural and microanalytical studies of sulfate attack. IV. Reactions of a slag cement paste with sodium and magnesium sulfate solutions, *Cem. Concr. Res.* 26 (7) (1996) 1013–1028.
- [3] H.F.W. Taylor, C. Famy, K.L. Scrivener, Delayed ettringite formation, *Cem. Concr. Res.* 31 (5) (2001) 683–693.
- [4] F.P. Glasser, Progress in the immobilization of radioactive wastes in cement, *Cem. Concr. Res.* 22 (2–3) (1992) 201–216.
- [5] T. Asano, T. Kawasaki, N. Higuchi, Y. Horikawa, Feasibility study of solidification for low-level liquid waste generated by sulfuric acid elution treatment of spent ion exchange resin, *J. Power Energy Syst.* 2 (1) (2008) 206–214.
- [6] N. Mobasher, H. Kinoshita, S.A. Bernal, C.A. Sharrad,  $\text{Ba}(\text{OH})_2$  – blast furnace slag composite binders for the encapsulation of sulphate bearing nuclear waste, *Adv. Appl. Ceram.* 113 (1) (2014) 42–49.
- [7] Y. Esen, B. Yilmazer, An investigation of X-ray and radio isotope energy absorption of heavyweight concretes containing barite, *Bull. Mater. Sci.* 34 (1) (2011) 169–175.
- [8] IAEA TRS402, Handling and Processing of Radioactive Waste for Nuclear Applications, Technical Reports Series, IAEA, Vienna, 2001.

- [9] N. Mobasher, S.A. Bernal, O.H. Hussain, D.C. Apperley, H. Kinoshita, J.L. Provis, Characterisation of  $\text{Ba}(\text{OH})_2\text{-Na}_2\text{SO}_4$ -blast furnace slag cement-like composites for the immobilisation of sulphate bearing nuclear wastes, *Cem. Concr. Res.* 66 (2014) 64–74.
- [10] J.L. Provis, S.A. Bernal, Geopolymers and related alkali-activated materials, *Annu. Rev. Mater. Res.* 44 (2014) 299–327.
- [11] Y. Bai, N. Collier, N. Milestone, C. Yang, The potential for using slags activated with near neutral salts as immobilisation matrices for nuclear wastes containing reactive metals, *J. Nucl. Mater.* 413 (3) (2011) 183–192.
- [12] M.L.D. Gougar, B.E. Scheetz, D.M. Roy, Ettringite and C-S-H Portland cement phases for waste ion immobilization: a review, *Waste Manag.* 16 (4) (1996) 295–303.
- [13] I. Akkurt, C. Basyigit, S. Kilincarslan, B. Mavi, The shielding of  $\gamma$ -rays by concretes produced with barite, *Prog. Nucl. Energy* 46 (1) (2005) 1–11.
- [14] I.G. Richardson, G.W. Groves, The incorporation of minor and trace elements into calcium silicate hydrate (C-S-H) gel in hardened cement pastes, *Cem. Concr. Res.* 23 (1) (1993) 131–138.
- [15] P. Bouniol, A. Aspart, Disappearance of oxygen in concrete under irradiation: the role of peroxides in radiolysis, *Cem. Concr. Res.* 28 (11) (1998) 1669–1681.
- [16] P.E. Pottier, F.P. Glasser, Characterization of Low and Medium-level Radioactive Waste Forms, Final report-2nd programme 1980-84, Commission of the European Communities, Luxembourg, 1986.
- [17] N. Mobasher, S.A. Bernal, H. Kinoshita, C.A. Sharrad, J.L. Provis, Gamma irradiation resistance of an early age slag-blended cement matrix for nuclear waste encapsulation, *J. Mater. Res.* 30 (9) (2015) 1563–1571.
- [18] F. Vodák, V. Vydra, K. Trtik, O. Kapickova, Effect of gamma irradiation on properties of hardened cement paste, *Mater. Struct.* 44 (2011) 101–107.
- [19] G. Bar-Nes, A. Katz, Y. Peled, Y. Zeiri, The combined effect of radiation and carbonation on the immobilization of Sr and Cs ions in cementitious pastes, *Mater. Struct.* 41 (2008) 1563–1570.
- [20] I. Richardson, G. Groves, C. Wilding, Effect of  $\gamma$ -radiation on the microstructure and microchemistry of GGBFS/OPC cement blends, *Mater. Res. Soc. Symp. Proc.* 176 (1989) 31–37.
- [21] J.D. Palmer, G.A. Fairhall, Properties of cement systems containing intermediate level wastes, *Cem. Concr. Res.* 22 (2–3) (1992) 325–330.
- [22] B. Craeeye, G. De Schutter, C. Vuye, I. Gerardy, Cement-waste interactions: hardening self-compacting mortar exposed to gamma radiation, *Prog. Nucl. Energy* 83 (2015) 212–219.
- [23] Y. Haruguchi-Yukitomo, T. Sato, M. Sasoh, M. Kaneko, Y. Yamashita, M. Obata, Cement solidification method for intermediate-level liquid waste containing sodium sulphate ( $\text{Na}_2\text{SO}_4$ ), Waste Management Conference (WM2009), Phoenix, AZ (2009).
- [24] A. Rashad, Y. Bai, P. Basheer, N. Milestone, N. Collier, Hydration and properties of sodium sulfate activated slag, *Cem. Concr. Compos.* 37 (2013) 20–29.
- [25] N. Mobasher, S.A. Bernal, J.L. Provis, Structural evolution of an alkali sulphate activated slag cement, *J. Nucl. Mater.* 468 (2016) 97–104.
- [26] R.J. Myers, S.A. Bernal, R. San Nicolas, J.L. Provis, Generalized structural description of calcium-sodium aluminosilicate hydrate gels: the cross-linked tobermorite model, *Langmuir* 17 (2013) 5294–5306.
- [27] N. Mobasher, S.A. Bernal, O.H. Hussein, D.C. Apperley, H. Kinoshita, J.L. Provis, Characterisation of  $\text{Ba}(\text{OH})_2\text{-Na}_2\text{SO}_4$ -blast furnace slag cement-like composites for the immobilisation of sulphate bearing nuclear wastes, *Cem. Concr. Res.* 66 (2014) 64–74.
- [28] N. Meller, K. Kyritsis, C. Hall, The hydrothermal decomposition of calcium monosulfoaluminate 14-hydrate to katoite hydrogarnet and  $\beta$ -anhydrite: an in-situ synchrotron X-ray diffraction study, *J. Solid State Chem.* 182 (2009) 2743–2747.
- [29] C.A. Utton, E. Gallucci, J. Hill, N.B. Milestone, Interaction between  $\text{BaCO}_3$  and OPC/BFS composite cements at 20°C and 60°C, *Cem. Concr. Res.* 41 (3) (2011) 236–243.
- [30] R.J. Kirkpatrick, MAS NMR-spectroscopy of minerals and glasses, *Rev. Mineral.* 18 (1988) 341–403.
- [31] M.D. Andersen, H.J. Jakobsen, J. Skibsted, A new aluminium-hydrate species in hydrated Portland cements characterized by  $^{27}\text{Al}$  and  $^{29}\text{Si}$  MAS NMR spectroscopy, *Cem. Concr. Res.* 36 (1) (2006) 3–17.
- [32] J. Skibsted, E. Henderson, H.J. Jakobsen, Characterization of calcium aluminate phases in cements by  $^{27}\text{Al}$  MAS NMR spectroscopy, *Inorg. Chem.* 32 (6) (1993) 1013–1027.
- [33] I.G. Richardson, A.R. Brough, G.W. Groves, C.M. Dobson, The characterization of hardened alkali-activated blast-furnace slag pastes and the nature of the calcium silicate hydrate (C-S-H) paste, *Cem. Concr. Res.* 24 (5) (1994) 813–829.
- [34] R.J. Myers, B. Lothenbach, S.A. Bernal, J.L. Provis, Thermodynamic modelling of alkali-activated slag cements, *Appl. Geochem.* 61 (2015) 233–247.
- [35] I.G. Richardson, A.R. Brough, R. Brydson, G.W. Groves, C.M. Dobson, Location of aluminum in substituted calcium silicate hydrate (C-S-H) gels as determined by  $^{29}\text{Si}$  and  $^{27}\text{Al}$  NMR and EELS, *J. Am. Ceram. Soc.* 76 (9) (1993) 2285–2288.
- [36] B. Lothenbach, F. Winnefeld, C. Alder, E. Wieland, P. Lunk, Effect of temperature on the pore solution, microstructure and hydration products of Portland cement pastes, *Cem. Concr. Res.* 37 (4) (2007) 483–491.
- [37] A.N. Christensen, T.R. Jensen, J.C. Hanson, Formation of ettringite,  $\text{Ca}_6\text{Al}_2(\text{SO}_4)_3(\text{OH})_{12} \cdot 26\text{H}_2\text{O}$ , Aft, and monosulfate,  $\text{Ca}_4\text{Al}_2\text{O}_6(\text{SO}_4) \cdot 14\text{H}_2\text{O}$ , AFm-14, in hydrothermal hydration of Portland cement and of calcium aluminum oxide—calcium sulfate dihydrate mixtures studied by in situ synchrotron X-ray powder diffraction, *J. Solid State Chem.* 177 (6) (2004) 1944–1951.
- [38] F. Glasser, D. Damidot, M. Atkins, Phase development in cement in relation to the secondary ettringite problem, *Adv. Cem. Res.* 7 (26) (1995) 57–68.
- [39] B. Lothenbach, T. Matschei, G. Möschner, F.P. Glasser, Thermodynamic modelling of the effect of temperature on the hydration and porosity of Portland cement, *Cem. Concr. Res.* 38 (1) (2008) 1–18.
- [40] B.A. Clark, P.W. Brown, The formation of calcium sulfoaluminate hydrate compounds Part II, *Cem. Concr. Res.* 30 (2000) 233–240.
- [41] R. Barbarulo, H. Peycelon, S. Prene, Experimental study and modelling of sulfate sorption on calcium silicate hydrates, *Ann. Chim. - Sci. Mater.* 28 (2003) 55–510.
- [42] J. Skibsted, E. Henderson, H.J. Jakobsen, Characterization of calcium aluminate phases in cements by  $^{27}\text{Al}$  MAS NMR spectroscopy, *Inorg. Chem.* 32 (6) (1993) 1013–1027.
- [43] R.J. Myers, S.A. Bernal, J.L. Provis, J.D. Gehman, J.S.J. van Deventer, The role of Al in cross-linking of alkali-activated slag cements, *J. Am. Ceram. Soc.* 98 (3) (2015) 996–1004.
- [44] R.J. Myers, E. L'Hôpital, J.L. Provis, B. Lothenbach, Effect of temperature and aluminium on calcium (alumino)silicate hydrate chemistry under equilibrium conditions, *Cem. Concr. Res.* 68 (2015) 83–93.
- [45] M.D. Andersen, H.J. Jakobsen, J. Skibsted, Incorporation of aluminum in the calcium silicate hydrate (C-S-H) of hydrated Portland cements: A high-field  $^{27}\text{Al}$  and  $^{29}\text{Si}$  MAS NMR investigation, *Inorg. Chem.* 42 (7) (2003) 2280–2287.
- [46] N. Mobasher, S.A. Bernal, J.L. Provis, Structural evolution of a sodium sulfate activated slag cement, *J. Nucl. Mater.* 468 (2016) 97–104.
- [47] S.A. Bernal, R. San Nicolas, R.J. Myers, R. Mejía de Gutiérrez, F. Puertas, J.S.J. van Deventer, J.L. Provis, MgO content of slag controls phase evolution and structural changes induced by accelerated carbonation in alkali-activated binders, *Cem. Concr. Res.* 57 (2014) 33–43.
- [48] Y. Shimada, J.F. Young, Structural changes during thermal dehydration of ettringite, *Adv. Cem. Res.* 13 (2) (2001) 77–81.
- [49] E. L'Hôpital, B. Lothenbach, K. Scrivener, D.A. Kulik, Alkali uptake in calcium alumina silicate hydrate (C-A-S-H), *Cem. Concr. Res.* 85 (2016) 122–136.
- [50] L. Alarcon-Ruiz, G. Platret, E. Massieu, A. Ehrlicher, The use of thermal analysis in assessing the effect of temperature on a cement paste, *Cem. Concr. Res.* 35 (3) (2005) 609–613.
- [51] B.Z. Dilnesa, B. Lothenbach, G. Renaudin, A. Wichser, D. Kulik, Synthesis and characterization of hydrogarnet  $\text{Ca}_3(\text{Al}_x\text{Fe}_{1-x})(\text{SiO}_4)_y(\text{OH})_{4(3-y)}$ , *Cem. Concr. Res.* 59 (2014) 96–111.
- [52] M. Ben Haha, G. Le Saout, F. Winnefeld, B. Lothenbach, Influence of activator type on hydration kinetics, hydrate assemblage and microstructural development of alkali activated blast-furnace slags, *Cem. Concr. Res.* 41 (3) (2011) 301–310.
- [53] G. Villain, M. Thiery, G. Platret, Measurement methods of carbonation profiles in concrete: thermogravimetry, chemical analysis and gammadensimetry, *Cem. Concr. Res.* 37 (2007) 1182–1192.
- [54] P. Bouniol, E. Bjergbakke, A comprehensive model to describe radiolytic processes in cement medium, *J. Nucl. Mater.* 372 (1) (2008) 1–15.
- [55] I. Akkurt, H. Akyildirim, B. Mavi, S. Kilincarslan, C. Basyigit, Gamma-ray shielding properties of concrete including barite at different energies, *Prog. Nucl. Energy* 52 (7) (2010) 620–623.